Virology 447 (2013) 131–139

Contents lists available at ScienceDirect

Virology

journal homepage: www.elsevier.com/locate/yviro

Rice black-streaked dwarf virus P10 induces membranous structures at the ER and elicits the unfolded protein response in *Nicotiana benthamiana*

Zongtao Sun [a], Di Yang [b], Li Xie [a], Liying Sun [a], Shanglin Zhang [b], Qisong Zhu [c], Junmin Li [a], Xu Wang [a], Jianping Chen [a,*]

[a] State Key Laboratory Breeding Base for Zhejiang Sustainable Pest and Disease Control, Ministry of Agriculture Key Laboratory of Biotechnology in Plant Protection, Zhejiang Provincial key laboratory of Plant Virology, Institute of Virology and Biotechnology, Zhejiang Academy of Agricultural Sciences, Hangzhou 310021, China
[b] College of Plant Protection, Anhui Agricultural University, Hefei 230036, China
[c] Shandong Rice Research Institute, Jinan 250100, China

ARTICLE INFO

Article history:
Received 29 March 2013
Returned to author for revisions
13 July 2013
Accepted 1 September 2013
Available online 24 September 2013

Keywords:
Rice black-streaked dwarf virus
Capsid protein P10
ER membrane modification
ER stress
Unfolded protein response

ABSTRACT

Endoplasmic reticular (ER) membrane modifications play an important role in viral RNA replication and virion assembly but little is known about the involvement of ER-membrane remodeling in the infection cycle of fijiviruses in plant cells. The subcellular localization of *Rice black-streaked dwarf virus* outer capsid P10 was therefore examined using live-cell imaging. P10 fused to eGFP formed vesicular structures associated with ER membranes in *Nicotiana benthamiana* epidermal cells and in rice protoplasts. Subcellular fractionation experiments confirmed that P10 is an integral membrane protein. Three predicted transmembrane domains and two less-well-defined domains were each able to target eGFP to the ER. Disruption of the actin cytoskeleton with LatB, indicated that the maintenance of P10-induced membrane structures required the intact actin cytoskeleton. P10 induced the expression of ER stress marker genes, including ER stress-related chaperones and transcription factor, indicating that RBSDV P10 triggers ER stress and the unfolded protein response.

Introduction

The endomembrane system, including the endoplasmic reticulum (ER), the Golgi apparatus, endosomes and other organelles, is essential for the synthesis, modification and transport of cellular proteins. Many RNA viruses are reported to use the endomembrane system for their replication, virion packaging, and intercellular transport (Grangeon et al., 2012; Verchot, 2011). Various membrane-derived structures, including spherules, membranous vesicles and/or multivesicular bodies can be found in virus-infected cells. These membrane modifications are believed to enhance replication efficiency, to provide a platform for virion assembly, and possibly to shield them from recognition by host defense responses (Laliberté and Sanfaçon, 2010). Virus-induced membranous vesicles are derived from different intracellular organelles in the host, depending on the virus. The ER is often modified by one or several viral membrane anchor proteins and utilized by many plant and animal viruses as a site of virus replication and virion assembly (Bamunusinghe et al., 2011; Zhang and Sanfaçon, 2006; Zhang et al., 2005). Viral membrane anchor proteins are usually integral membrane proteins and have the ability to associate with the ER in the absence of other viral proteins. Exogenous expression of viral proteins individually has been used to investigate the role of these proteins in membrane association with ER. For example, the 1a protein of Brome mosaic virus (BMV) was shown to induce ER-derived membranous spherules (Chen and Ahlquist, 2000). Similar effects were caused by the 32-kDa protein of Cowpea mosaic virus (CPMV) (Carette et al., 2000) and the NTB-VPg and X2 proteins of Tomato ringspot nepovirus (ToRSV) (Zhang and Sanfaçon, 2006). Various ER membrane-binding domains, including transmembrane hydrophobic helices, amphipathic helices, and other less-well-defined elements, were identified in these membrane anchor proteins.

Reoviruses are double-stranded RNA viruses with multiple genome components. Within the large family *Reoviridae*, plant-infecting viruses are found in the genera *Phytoreovirus*, *Fijivirus* and *Oryzavirus*. *Rice black-streaked dwarf virus* (RBSDV), belonging to the genus *Fijivirus*, can seriously affect the production of rice and maize. RBSDV is propagatively transmitted to rice, maize, barley and wheat in a persistent manner by the small brown

* Corresponding author. Fax: +86 571 8640 4258.
E-mail address: Jpchen2001@126.com (J. Chen).

0042-6822/$ - see front matter © 2013 Elsevier Inc. All rights reserved.
http://dx.doi.org/10.1016/j.virol.2013.09.001

planthopper (*Laodelphax striatellus*). RBSDV-infected plants become stunted and have growth abnormalities. RBSDV has 10 genomic segments of double stranded RNA and icosahedral virions which are 65–70 nm in diameter (Zhang et al., 2001). The genome is encapsidated by two protein shells, one outer capsid and one inner core shell. Viral replication and packaging have been well studied in several animal-infecting reoviruses, including rotaviruses and other mammalian reoviruses (Reinisch et al., 2000; Trask et al., 2012a). In animal-infecting reoviruses, the outer capsids are removed by endosomal proteases during entry into host cells, releasing core particles into the cytoplasm. The capped viral plus-strand RNAs are then released into the cytoplasm for translation into viral proteins. Distinct viral structures, viroplasms, are formed in the cytoplasm by a nonstructural protein. These dynamic and highly organized structures direct the packaging and replication of the viral genome into progeny viral core particles. The core particles are then packaged into the double-layered virus particles under the action of outer capsid proteins. Accumulated information supports the involvement of the endomembrane system in this packaging in various members of the *Reoviridae* (Coffey et al., 2006; Trask et al., 2012b). Rotavirus outer capsid protein VP7 localizes in the ER membrane, and facilitates the migration of the intermediates from the viral factory to ER in final capsid assembly (Maass and Atkinson, 1994; Trask et al., 2012a). Mammalian reovirus outer capsid protein μ1 localizes to lipid droplets, ER, and mitochondria (Coffey et al., 2006). Previous studies showed that RBSDV P10 specifically reacts with a protein component located on the outer shell of the virus particle and serves as a major outer capsid protein (Isogai et al., 1998). Liu et al. reported that RBSDV P10 has self-interacting properties and forms oligomeric complexes in solution (Liu et al., 2007). However, detailed information about the RBSDV outer capsid proteins is still not known and their involvement with ER modification or ER stress has not been investigated.

In this study, confocal laser scanning microscope (CLSM) was used to explore the subcellular localization of RBSDV outer capsid P10 in *Nicotiana benthamiana* epidermal cells and in rice protoplasts. We show that transmembrane domains in P10 mediate its targeting to ER where it forms membrane-associated structures, and that this process requires the integrity of the actin cytoskeleton. We also found that heterologous expression of P10 induces ER stress and the Unfolded Protein Response (UPR).

Results

Subcellular localization of RBSDV outer capsid P10 in N. benthamiana leaves and in rice protoplasts

P10 was fused to the N-terminus of enhanced green fluorescent protein (eGFP) under the control of the CaMV 35S promoter. The P10-eGFP construct was transiently expressed in *N. benthamiana* epidermal cells by agroinfiltration and GFP fluorescence in the inoculated leaves was examined by confocal fluorescence microscopy 2 days post-infiltration (dpi). In the controls, free eGFP was present in the cytosol and nucleus (Fig. 1A, panel I), as described previously (Sun et al., 2013), but where P10-eGFP was expressed, in addition to the fluorescence in nucleus (Fig. S1), there were fluorescent circular structures in the cytosol (Fig. 1A, panel II). These circular structures appeared as single or multiple aggregations and those in the cytosol were associated with a characteristic reticular network, which seemed to be the typical cortical ER network. To determine whether these structures assemble at the ER network, the co-localization of P10-eGFP and an ER marker fused to mCherry was examined. In epidermal cells expressing ER:mCherry alone, the fluorescence was detected in the typical stationary cortical ER network (Fig. 1A, panel III) as expected and as reported previously (Nelson et al., 2007). When P10-eGFP was co-expressed with ER:mCherry (Fig. 1B), there was co-labeling, suggesting that P10-eGFP forms the circular structures at the ER membrane in *N. benthamiana* epidermal cells.

In order to investigate P10 fusion associated with ER in the natural rice host, the plasmids P10-eGFP and ER:mCherry were co-transformed into rice protoplasts. As shown in Figs. 2A and B, the fluorescence of P10-eGFP (panel I) coincided with that of ER:mCherry (panel II) in the cytosol, and the circular structures formed by P10-eGFP were co-labeled with ER marker. These results indicate that P10-eGFP forms the circular structures at the ER membrane in both *N. benthamiana* epidermal cells and in rice protoplasts.

Transmembrane prediction and subcellular fractionation of P10

The RBSDV P10 protein has 558 amino acids and a molecular-weight of about 60 kDa. Bioinformatics analyses revealed that P10 has three predicted transmembrane domains (TM1, TM2 and TM3) (Table S1), although the exact borders of the predicted transmembrane helices differed among different methods. These predicted transmembrane domains share the consensus hydrophobic cores that mainly contain hydrophobic residues (A, I, V, L, and F) (Fig. 3A). Subcellular fractionation of the plant tissue extracts expressing RBSDV P10-eGFP was performed to verify the computer predictions. The plant tissue expressing P10-eGFP was lysed, and extracts were separated by high-speed centrifugation into pellet (P30) and supernatant (S30) fractions. An immunoblot analysis revealed that P10 was present in the pellet fraction (P30) (Fig. 3B) which contains membrane-derived microsomes. The P30 fraction was further treated by either 1 M KCl, 0.1 M Na_2CO_3 (pH 11), 4 M Urea or lysis buffer containing 1% Triton X-100. The chemical treatments with KCl, Na_2CO_3 and Urea are known to release peripheral membrane proteins from the membranes but not integral membrane proteins, while the detergent Triton X-100 releases integral membrane proteins. After treatment with 1 M KCl, 0.1 M Na_2CO_3 (pH 11) or 4 M Urea, P10 remained in the P30 fraction, but after Triton X-100 treatment P10 was found in the supernatant fraction (Fig. 3C). Taken together, these results indicate that P10 is an integral membrane protein.

RBSDV P10 contains multiple ER-targeting domains

P10 mutants were then constructed to investigate the membrane targeting sequences in more detail. We first generated four mutants of P10-eGFP in which the predicted transmembrane helices TM1, TM2, and TM3 were deleted either individually or in combination (Fig. 4A, mutants designated as dTM1, dTM2, dTM3, and dTM123). All four P10 derivatives retained the ability to associate with the ER (Fig. 5). To provide further evidence that these mutants were associated with the ER membrane, sucrose density gradient centrifugation was employed in the presence of 3 mM $MgCl_2$. The control GFP in the cytosol appered in fractions 1–2, while the peaks of ER:GFP and P10-GFP were in fractions 3–5 (Fig. 4B). This distribution pattern is consistent with previous reports (Schaad et al., 1997; Wienecke et al., 1982) that the ER membrane is found at 30–40% sucrose in the presence of 3 mM $MgCl_2$. Membrane flotation assays showed that the distribution pattern of mutant dTM123 was similar to that of P10-GFP and ER:GFP (Fig. 4B). We then examined the transmembrane helices individually by fusing TM1, TM2, or TM3 alone to the N terminus of eGFP in a transient expression vector (Fig. 4A; TM1, TM2 and TM3). As shown in Fig. 5, these transmembrane helices each targeted the ER. They were also partitioned to membrane-enriched fractions in subcellular fractionation experiments (Fig. 4B). We therefore concluded

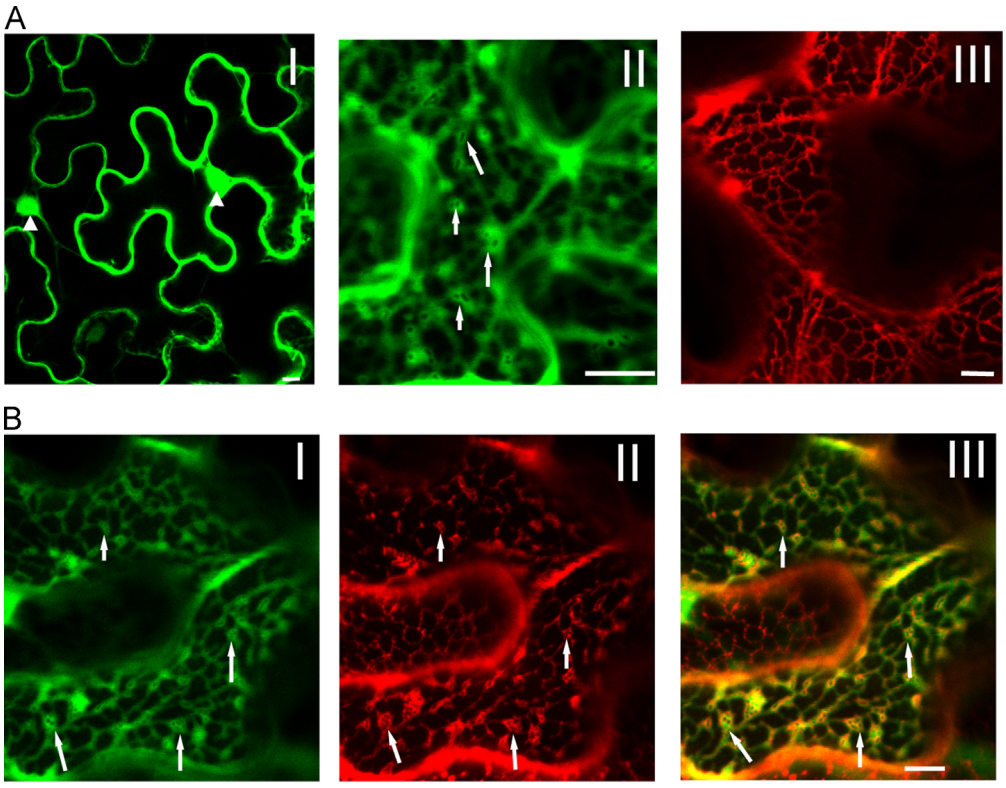

Fig. 1. Subcellular localization of RBSDV P10-eGFP in agroinfiltrated *N. benthamiana* leaf cells. (A) Confocal images of eGFP (panel I), P10-eGFP (panel II) and ER:mCherry (panel III). The white triangle in panel I indicates the nucleus stained by eGFP. The arrows in panel II show the single or multiple circular structures induced by RBSDV P10-eGFP in *N. benthamiana* epidermal cells. (B) confocal images of cells co-expressing P10-eGFP (panel I) and ER:mCherry (panel II). The arrows in these panels indicate that the circular structures induced by P10-eGFP are located at the ER. Bars, 10 μm.

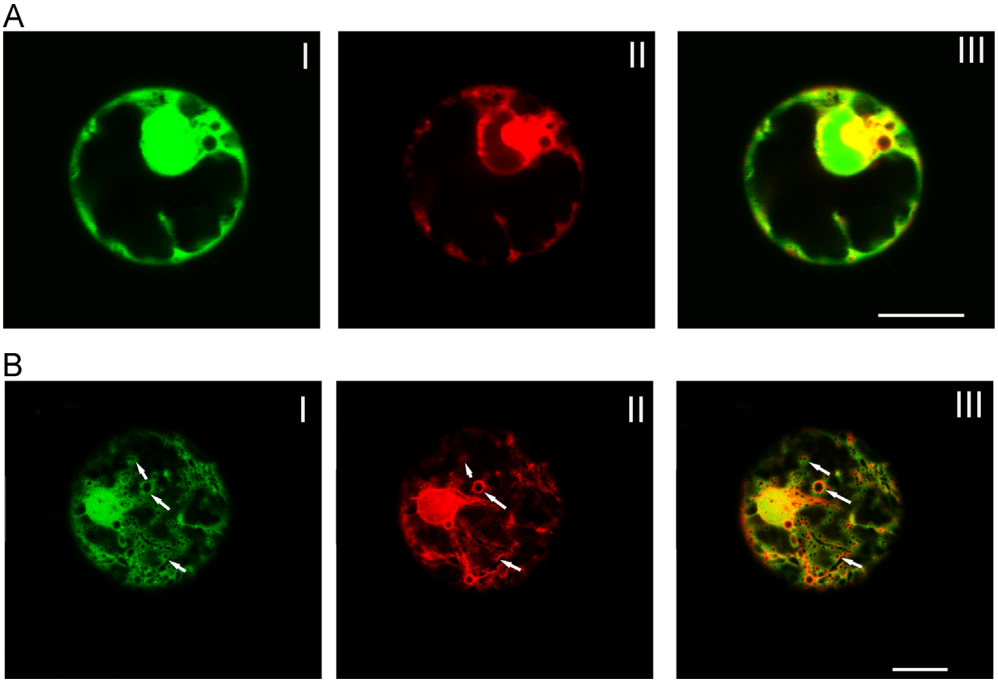

Fig. 2. Analysis of P10-eGFP localization in rice protoplasts. (A and B) Show P10-eGFP (panel I) and ER:mCherry (panel II) coexpression in rice protoplasts in different sections, respectively. The arrows in these panels indicate that the circular structures induced by P10-eGFP are located at the ER. Bars, 10 μm.

that in addition to the three predicted transmembrane helices other uncharacterized domains were also responsible for P10 ER-targeting. We then fused different portions of P10 (Fig. 4A; constructs 1-110, 140-240, 270-480, and 500-558) to the N terminus of eGFP and tested whether any of these could associate with the ER. The 120-240 and 500-558 fusions were exclusively located in the polygonal and tubular network of the ER (Fig. 5). These two mutants were present in fractions 3–5 in membrane flotation assays (Fig. 4B), confirming that they are membrane-associated. In contrast, most of the 1-110 fusion formed large aggregates in the cytosol and the fluorescence of these

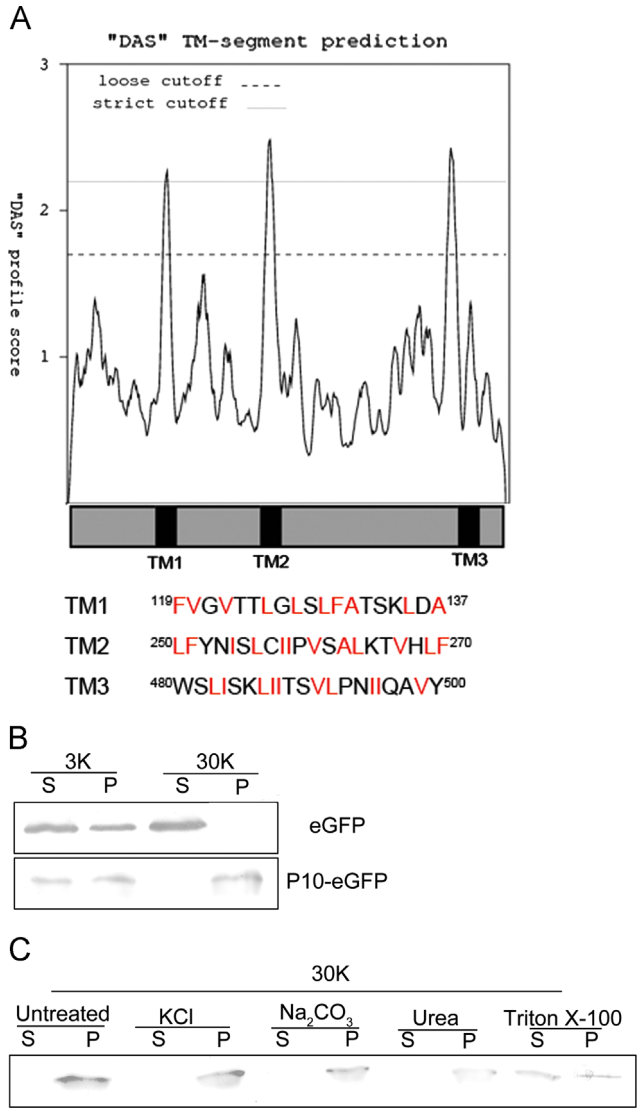

Fig. 3. Bioinformatics analysis and subcellular fractionation of RBSDV P10. (A) The DAS analysis clearly shows three transmembrane helices in P10. Scores in the vertical axis indicate the value of the putative transmembrane helices (1.7, loose cutoff; 2.2, strict cutoff). Numbers on the horizontal axis indicate the relative amino acid positions in the P10 protein. The hydrophobic residues (A, I, V, L, and F) in these transmembrane helices are labeled in red. (B and C) Subcellular fractionation of P10 fusion proteins. Plant tissues expressing P10-eGFP or eGFP were fractionated into soluble (S) and membrane-enriched (P) fractions as described in Materials and Methods. 3K, the extracts following centrifugation at 3000*g*; 30K, the extracts following centrifugation at 30,000*g*; the samples treated or untreated with the chemicals are also marked.

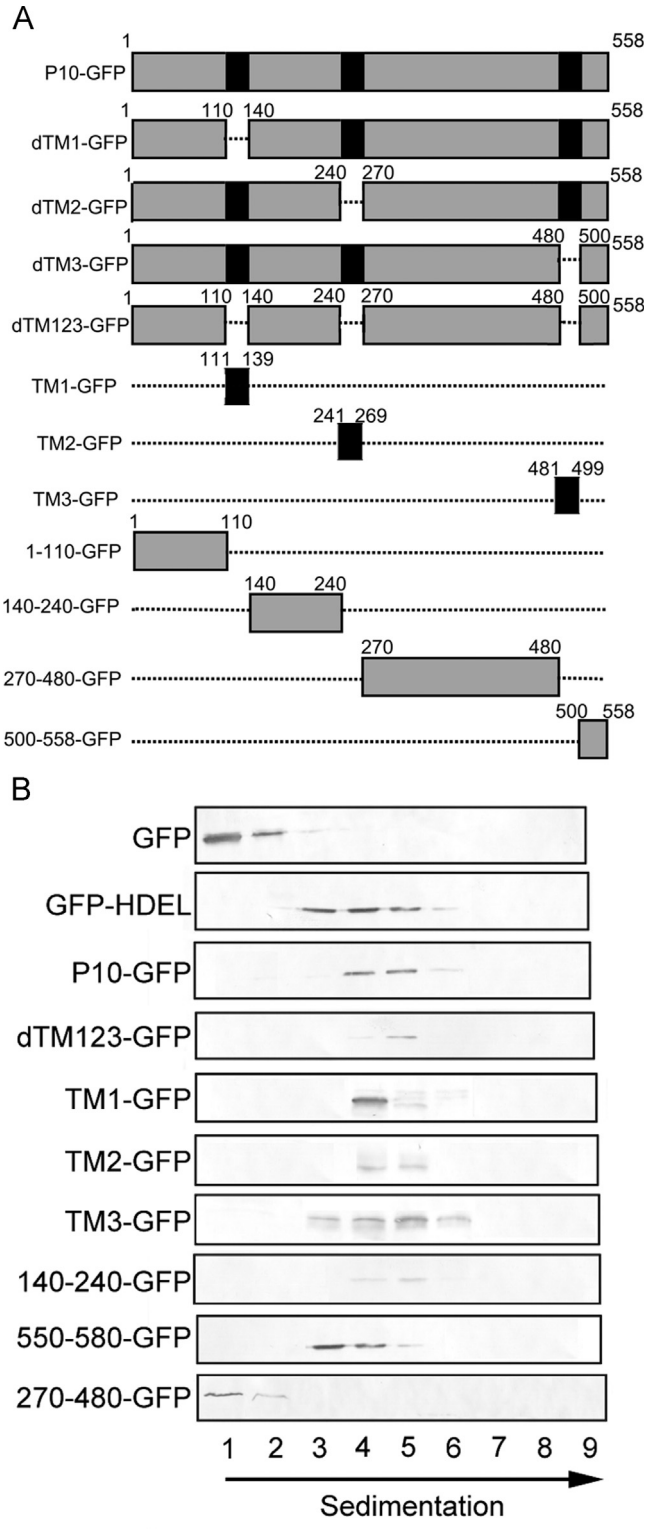

Fig. 4. RBSDV P10 mutant analysis and membrane flotation assays. (A) The transmembrane helices (TM1, TM2 and TM3) are colored black. Blocks represent regions of the P10 protein contained in the construct. Discontinuous dots represent the deleted region. Numbers indicate the relative amino acid positions in the RBSDV P10 protein. (B) Immunoblot analyses of the protein extracts following separation in the sucrose gradients as described in Materials and Methods, with the fraction numbers shown at the bottom.

aggregates was associated with chloroplasts (Figs. 5 and 6). The fluorescence of the 270-480 fusion was diffusely distributed in the cytoplasm and the nucleus (Fig. 5) and this fusion protein was present in the top of the gradient in membrane flotation assays, confirming that it was not membrane-associated. Taken together, these results suggested that two uncharacterized regions (120-240 and 500-558) have the ability to target ER even though they were not identified as transmembrane domains by existing programs.

The ER-membrane associated structures formed by P10 were dependent on actin microfilaments

Previous studies revealed that the ER network and its extensive mobility were associated with the actin cytoskeleton (Liebe and Menzel, 1995). To determine whether the P10-induced ER-membrane associated structures were affected by disrupting the actin cytoskeleton, the leaves were treated twice with 10 μM latrunculin B (LatB)

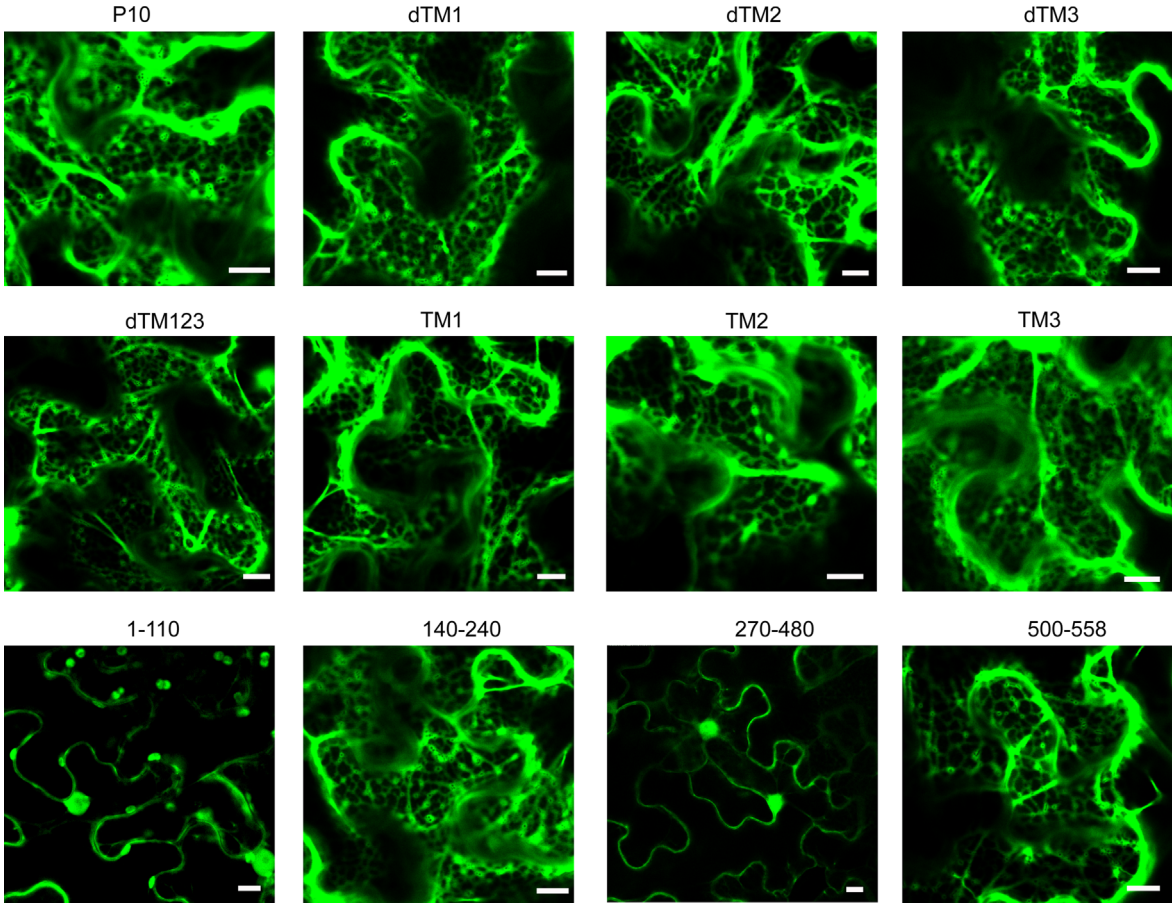

Fig. 5. Effects of RBSDV P10 mutants on ER-targeting in *N. benthamiana* leaf cells. Subcellular localization of P10-GFP derivatives in epidermal cells of *N. benthamiana*. GFP fusions were expressed in leaves of *N. benthamiana* by agroinfiltration. Epidermal cells were examined 3 days after agroinfiltration by confocal microscopy. Bars, 10 μm.

Fig. 6. Subcellular localization of 1-110 fusion in agroinfiltrated *N. benthamiana* leaf cells. 1-110 fusion was expressed in leaves of *N. benthamiana* by agroinfiltration as described in Materials and Methods. The arrows indicate the co-localization of the 1-110-eGFP fluorescence (green) and the auto-fluorescence of chloroplasts (red) resulting in a yellow color. Bars, 10 μm.

(once at the time of agroinfiltration and again 12 h prior to observation). LatB is known to depolymerize filamentous actin in eukaryotic cells. In LatB-treated leaves, RFP:Talin was redistributed to form aberrant aggregates as reported previously (Sun et al., 2013). As shown in Fig. 7A and B, the typical cortical ER network was disrupted after LatB treatment. These results confirmed that the ER network is supported by the actin cytoskeleton as reported previously (Avisar et al., 2008). In LatB-treated leaves, the fluorescence of P10-eGFP accumulated in the aberrant aggregates and was diffusely distributed in the cytosol whereas the P10-induced membrane structures were observed in the mock-treated DMSO leaves (Fig. 7C and D). These results indicate that P10-induced membrane structures required the intact actin cytoskeleton.

P10 induces the expression of ER stress-related chaperones and transcription factor

In eukaryotes, the ER is the processing factory for proteins destined for secretion or membrane insertion. During virus infection, substantial amounts of viral proteins are produced. Some of them are heavily modified transmembrane proteins. This raises the possibility that the accumulation of nascent and unfolded viral proteins in the lumen of ER might rapidly exceed its folding capacity, thereby perturbing the normal cellular function of ER. The disruption of ER homeostasis will result in the aggregation of unfolded or malformed proteins and elicit the UPR response (Zhang and Wang, 2012). To determine whether P10 induces ER

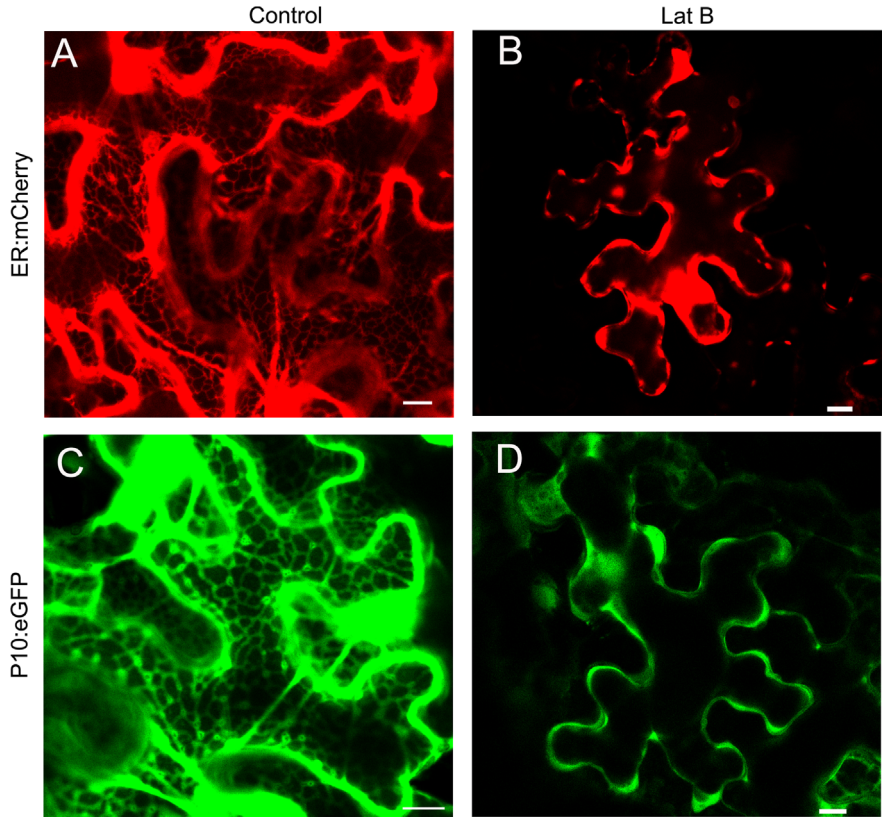

Fig. 7. The actin microfilaments are required for the maintenance of P10-induced circular structures. Confocal images of cells expressing ER:mCherry and P10-eGFP treated with DMSO (Control) or LatB, respectively. Note that the fluorescence of ER:mCherry and P10-eGFP accumulates in aberrant aggregates and is diffusely distributed in the cytosol in LatB-treated leaves, respectively. Bars, 10 μm.

stress and the UPR response, the transcript levels of ER stress marker genes *BiP*, *PDI*, *CAM* and *bZIP60*, were evaluated in *N. benthamiana*.

P10 and its mutant 1-110 were expressed under the control of the CaMV 35S promoter by agroinfiltration into *N. benthamiana* leaves. Mutant 1-110 was not associated with ER (Fig. 5), so it acted as a negative control. PVX TGBp3 can up-regulate the ER-resident chaperones and elicit the UPR in *Arabidopsis* and *N. benthamiana* (Ye et al., 2011, 2013), so it acted as a positive control. The total RNA of *N. benthamiana* leaves was extracted 2d post infiltration, and qRT-PCR was carried out. As shown in Fig. 8, the expression of 35S:P10 and 35S:TGBp3 resulted in about 2.5–3.5 fold higher levels of *BiP*, *PDI*, *CAM* and *bZIP60* transcript accumulation in comparison with the controls (the binary vector and the mutant 1-110) ($P < 0.05$). These data show that expression of P10 increases the expression of UPR-related chaperones and that P10 induces ER stress and the UPR in *N. benthamiana* leaves.

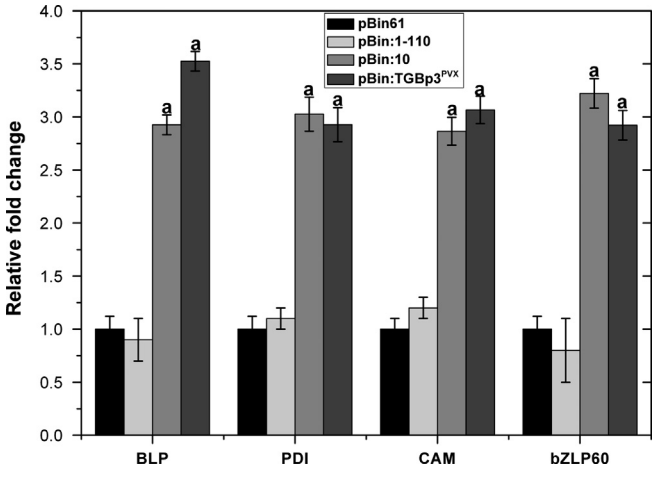

Fig. 8. RBSDV P10 induction of BiP, PDI, CAM and bZIP60 transcripts following agroinfiltration. Quantitative reverse-transcriptase polymerase chain reaction (qRT-PCR) of BiP, PDI, CAM and bZIP60 transcripts in *N. benthamiana* leaves expressing pBin61, pBin:1-110, pBin:P10 and pBin:TGBp3^{PVX}. Values represent averages of three replicate samples. Error bars represent the standard deviation from three independent experiments. The 'a' above the columns indicates a significant difference ($P < 0.05$) from the controls as assessed by Student's *t*-test.

Discussion

Detailed studies of RBSDV in plants are hampered by difficulties in maintaining host plants in the greenhouse and in using the insect vector to transmit it. Transient expression of viral proteins fused to fluorescent protein in the model plant *N. benthamiana* has proved to be a useful alternative method to study RBSDV protein functions. Using live imaging technology, the effects of the endomembrane system and cytoskeleton components on the subcellular localization of viral protein can be clearly observed (Held et al., 2008). In this study, our results showed that the P10 fusion formed membrane-associated circular structures in *N. benthamiana* epidermal cells and in rice protoplasts. Co-localization with an ER marker and subcellular fractionation showed that these P10-induced circular structures were associated with ER membranes. The fluorescence of P10 fusion also co-localized with ER:mCherry in rice protoplasts showing that *N. benthamiana* epidermal cells provide a suitable model system for transient expression experiments.

The ER may play a role in the replication cycle of fijiviruses as it does in rotaviruses (also belonging to the family *Reoviridae*).

In rotaviruses, the viral factories direct the packaging and replication of the viral genome into early capsid assembly intermediates. Migration of the intermediates to the endoplasmic reticulum (ER) and assembly of the ER-resident outer capsid protein VP7 results in the formation of intact virus particles (Trask et al., 2012b). For RBSDV, we assume that outer capsid protein P10 is retained in the ER to assemble the intermediates exiting from the viroplasms. This assumption is supported by immunoelectron microscopy of RBSDV-infected plant cells (Fig. S2). In white tumors of maize plants infected by RBSDV, intermediate virus particles were present in the viroplasms while the intact virions were seen just outside (Fig. S2). A similar phenomenon was observed in insect vector cells infected with rice ragged stunt virus (genus *Oryzavirus*) (Jia et al., 2012). These results indicate that the viroplasms are the site of the assembly of the intermediates, but not the site of assembly of intact virions. It therefore seems likely that the ER may be a scaffold for RBSDV capsid assembly, and that these ER-derived structures induced by P10 may facilitate capsid assembly at the ER.

Predictions that RBSDV P10 contains three transmembrane domains (TMs) (Table S1) were confirmed when, after fusion to eGFP, they showed a typical ER-associated distribution pattern (Fig. 5). Although these TMs act as membrane anchors to the ER, two uncharacterized domains (140-240 and 500-558) were also responsible for P10 ER-targeting (Fig. 5). These two regions were not predicted to contain transmembrane domains but an amphipathic helix is predicted in the 500-558 region (Fig. S3). Amphipathic helices are responsible for ER-targeting of many viral proteins (Liu et al., 2009; Zhang et al., 2005). An amphipathic helix of BMV protein 1a is essential for ER membrane association and perinuclear ER localization, and deletion or mutation of the amphipathic helix inhibits ER membrane association and abolishes RNA replication (Liu et al., 2009). The N-terminal amphipathic helix of tomato ringspot nepovirus NTB-VPg protein was necessary and sufficient for its ER membrane association (Zhang et al., 2005). Two amphipathic α-helices within a carboxyl-terminal domain are key determinants for the distribution pattern of mammalian reovirus outer capsid protein μ1 (Coffey et al., 2006). For RBSDV P10, the putative amphipathic helix may be responsible for the translocation of the C terminus of the protein into the ER lumen. Further experiments will examine the role of the C-terminal amphipathic helix on P10 membrane association and the ER-targeting element in the120-240 region. Interestingly, the N-terminal domain (1-110) fusion was associated with chloroplasts although the full length P10 fusion was not targeted to chloroplasts. The mammalian reovirus coat protein μ1 is autolytically cleaved into N-terminal (μ1N, residues 2–42) and C-terminal (μ1C) fragments during entry into host cells. Reovirus infectivity depends upon a process of membrane perforation involving the cleaved μ1N peptide. We speculate that the N terminus of RBSDV P10 may also be cleaved during the infection process. The role of the N terminus of P10 and the chloroplast-targeting signal will be investigated further.

ER is a spatially continuous component throughout the cytoplasm. Remodeling of the ER network, which consists of cisternae and interconnected membrane tubes, depends on the actin cytoskeleton in plant cells (Sparkes et al., 2009). In this study, ER-associated vesicular structures induced by P10 were inhibited by disruption of actin microfilaments with LatB treatment. We therefore conclude that the maintenance of P10-induced membrane structures at the ER requires the integrity of actin microfilaments.

The extensive use of intracellular membranes for the generation of viral replication complexes and for the assembly of virus particles likely overloads the ER during the viral infection (Zhang and Wang, 2012). A persistent stress on ER will trigger the ER stress-induced programmed cell death (PCD). To survive ER stress, viruses have developed different strategies to modulate the UPR as demonstrated by several animal viruses (Chan et al., 2006; Chan and Egan, 2005; Isler et al., 2005; Su et al., 2002). In plants, PVX TGBp3 can up-regulate the ER-resident chaperones and elicit the UPR in *Arabidopsis* and *N. benthamiana* (Ye et al., 2011, 2013). In this study, we showed that the ER chaperones (BiP, PDI and CAM) and ER stress-inducing transcription factor (bZIP60) were all up-regulated in tobacco leaves expressing P10. These results demonstrate that the heterologous expression of P10 elicited ER stress and the UPR in *N. benthamiana*. The modulation of the UPR has been reported in some mammalian rotaviruses and other reoviruses (Smith et al., 2006; Trujillo-Alonso et al., 2011; Xu et al., 1998). The activation of the cellular UPR and its modulation by these viruses was thought to be beneficial for viral replication and virion assembly, although the exact UPR pathway was not clear. For RBSDV, viral proteins are thought to migrate into the lumen of the ER for virion assembly, and we therefore speculate that P10 might modulate ER stress and the UPR to facilitate RBSDV capsid assembly by increasing the ER folding capacity.

Methods

Cloning and vector construction

For transient gene expression, Segment S10 was amplified and cloned into the binary vector pBin61 (Voinnet et al., 2000) between *BamH*I and *Sma*I sites to form pBin:P10. The same method was applied for constructing pBin:TGBp3^{PVX}. To construct fluorescent fusions, Segment S10 was amplified and cloned into pCV-eGFP-N1 (Lu et al., 2011) to form pCV-P10-eGFP.

A series of RBSDV P10 deletion and truncation mutants were constructed. The truncated fragment of S10 encoding amino acids 1-110, 111-139 (TM1), 140-240, 241-269 (TM2), 270-480, 481-499 (TM3), and 500-558 were amplified from the template pCV-P10-eGFP. The resulting PCR products were cloned into pGEMT-Easy, and then moved to binary vector pCV-eGFP-N1 to yield vectors expressing P10 truncations fused with eGFP. The P10 deletion derivatives (dTM1, dTM2, dTM3 and dTM123) were constructed using the KOD-Plus-Mutagenesis Kit (Toyobo). Similar strategies were used to generate the constructs expressing P10 deletion derivatives fused with eGFP. All primer sequences are available upon request. The sequence integrity of all deletion mutants was confirmed by sequencing.

Bioinformatics analysis of secondary structure and transmembrane helices

Transmembrane helices of P10 were predicted by the following programs using their default parameters: DAS (Cserzö et al., 1997), TMPred (Hofman, 1993), TopPRED (Claros and von Heijne, 1994), SPLIT (Juretić et al., 1993) and HMMTOP (Tusnady and Simon, 2001).

Agrobacterium tumefaciens-mediated transient expression in N. benthamiana

Transient expression assays on *N. benthamiana* plants were performed as previously described (Sun et al., 2013). Briefly, the recombinant binary constructs were introduced into *A. tumefaciens* strain GV3101 by electroporation. Transformed bacteria were grown overnight at 28 °C. The cultures were collected and re-suspended using an agroinfiltration buffer (10 mM $MgCl_2$, 10 mM morpholineethanesulfonic acid, pH 5.6, and 150 μM acetosyringone). The suspensions were adjusted to an optical density of 0.5 at 600 nm ($OD_{600\ nm}$) before leaf infiltration. For co-localization

experiments requiring the simultaneous expression of two different proteins, the individual cultures were adjusted to $OD_{600\ nm}=1$ and equal volumes were mixed before leaf infiltration. The cell suspensions were infiltrated into 4- to 6-week old *N. benthamiana* leaves.

Laser confocal microscopy and co-localization assays

Expression of fluorescent proteins was observed 36 h post-agroinfiltration. Leaf pieces of fresh leaves of *N. benthamiana* were examined with a Leica TCS SP5 confocal laser scanning microscope system (Leica Microsystems, Bannockburn, IL, USA). An argon laser was used to excite GFP at 488 nm and emission was monitored at 500–520 nm. mCherry was excited at 568 nm and emission was detected at 570–600 nm. Autofluorescence of chloroplasts was detected by using a 670 nm emission filter. Images were captured digitally and handled using the Leica LCS software and were further processed using Adobe Photoshop version 7.0 software (Adobe Systems Inc., San Jose, CA, USA).

Subcellular fractionation and membrane flotation assays

Subcellular fractionation and immunoblotting were performed as previously described (Genoves et al., 2011; Peremyslov et al., 2004). Briefly, leaf tissue (2 g) of *N. benthamiana* leaves transiently expressing either pCV-eGFP or pCV-P10-eGFP was ground with 5 ml of lysis buffer [20 mM HEPES, pH 6.8, 150 mM potassium acetate, 250 mM mannitol, and 1 mM $MgCl_2$]. After extraction, the homogenates were centrifuged at 3000*g* for 10 min to remove large cellular debris and the resulting supernatant was ultracentrifuged at 30,000*g* for 1 h to generate the soluble (S30) and the microsomal (P30) fractions. Then, the P30 fraction was treated with an equal volume of 1 M KCl, 0.1 M Na_2CO_3 (pH 11), 4 M Urea or lysis buffer containing 1% Triton X-100. After incubation for 1 h on ice, the samples were centrifuged at 30,000*g* for 1 h. The resulting pellet was re-suspended in lysis buffer. All fractions were prepared and boiled in sodium dodecyl sulfate-polyacrylamide gel electrophoresis (SDS-PAGE) sample buffer. Immunoblot analyses were done using mouse monoclonal antibodies to RBSDV P10 (a gift from Jianxiang Wu), or green fluorescent protein (GFP) (Roche).

Membrane flotation assays were conducted essentially as described previously (Schaad et al., 1997; Wienecke et al., 1982). Plant material was harvested and ground in lysis buffer containing 3 mM $MgCl_2$. S3 prepared as described above was loaded on top of 20–60% linear sucrose gradients containing 3 mM $MgCl_2$. Gradients were centrifuged for 20 h at 100,000*g* in a Beckman SWTi50 rotor at 4 °C, and 15 fractions were collected starting from the top. The fractions were subjected to immunoblot analysis after 12.5% polyacrylamide gel electrophoresis.

qRT-PCR experiments

Total RNA was extracted using Trizol reagent (Invitrogen) according to the manufacturer's instructions, followed by precipitation with lithium chloride and an additional phenol–chloroform extraction and ethanol precipitation. Genomic DNA was eliminated by treating each sample with RNase-free DNase I (Toyobo). First strand synthesis was performed using SuperScript III (Invitrogen) and random hexamer primers. Real-time PCR was then conducted using SYBR Green Mix (Promega) according to the manufacturer's instructions. Primers were used for the amplification of the targets, and efficiencies of all primers were verified by normal RT-PCR, gel electrophoresis and melting curve analysis. Reactions were conducted in triplicate. The comparative CT method employs the equation $2^{-\Delta\Delta CT}$, where the values of the endogenous control (18S RNA) and calibrator (a constant quantity of a healthy sample template) are subtracted from the target sample value to provide the ddCT value. The equation $2^{-\Delta\Delta CT}$ represents the fold of RNA accumulation.

Acknowledgments

The authors are indebted to Keke Yi (Zhejiang Academy of Agricultural Sciences, China) for ER:Cherry and to Jianxiang Wu (Zhejiang University, China) for P10 monoclonal antibody. We thank Ying Zhu and Lian Duan for preparation of rice protoplasts. We thank Mike Adams for critically reading the manuscript. This work was financially supported by the State Basic Research Program of China (2014CB138403, 2010CB126203 and 2012CB722504), the International Science & Technology Cooperation Program of China (2012DFA30900), the National Natural Science Foundation of China (31071660 and 31301637), Zhejiang Provincial Natural Science Foundation of China (Q13C140009), Zhejiang Provincial Postdoctoral Research Project Preferential Foundation (Bsh1202085), the Program for Zhejiang Leading Team of Science and Technology Innovation (2009R50032) and the Program for Leading Team of Agricultural Research and Innovation of Ministry of Agriculture, China.

Appendix A. Supplementary material

Supplementary data associated with this article can be found in the online version at http://dx.doi.org/10.1016/j.virol.2013.09.001.

References

Avisar, D., Prokhnevsky, A.I., Makarova, K.S., Koonin, E.V., Dolja, V.V., 2008. Myosin XI-K is required for rapid trafficking of Golgi stacks, peroxisomes, and mitochondria in leaf cells of *Nicotiana benthamiana*. Plant Physiol. 146, 1098–1108.

Bamunusinghe, D., Seo, J.-K., Rao, A.L.N., 2011. Subcellular localization and rearrangement of endoplasmic reticulum by *brome mosaic virus* capsid protein. J. Virol. 85, 2953–2963.

Carette, J.E., Stuiver, M., Van Lent, J., Wellink, J., Van Kammen, A., 2000. *Cowpea mosaic virus* infection induces a massive proliferation of endoplasmic reticulum but not Golgi membranes and is dependent on de novo membrane synthesis. J. Virol. 74, 6556–6563.

Chan, C.P., Siu, K.L., Chin, K.T., Yuen, K.Y., Zheng, B., Jin, D.Y., 2006. Modulation of the unfolded protein response by the severe acute respiratory syndrome coronavirus spike protein. J. Virol. 80, 9279–9287.

Chan, S.W., Egan, P.A., 2005. Hepatitis C virus envelope proteins regulate CHOP via induction of the unfolded protein response. FASEB J. 19, 1510–1512.

Chen, J., Ahlquist, P., 2000. *Brome mosaic virus* polymerase-like protein 2a is directed to the endoplasmic reticulum by helicase-like viral protein 1a. J. Virol. 74, 4310–4318.

Claros, M., von Heijne, G., 1994. TopPred II: an improved software for membrane protein structure predictions. Comput. Appl. Biosci. 10, 685–686.

Coffey, C.M., Sheh, A., Kim, I.S., Chandran, K., Nibert, M.L., Parker, J.S.L., 2006. Reovirus outer capsid protein μ1 induces apoptosis and associates with lipid droplets, endoplasmic reticulum, and mitochondria. J. Virol. 80, 8422–8438.

Cserzö, M., Wallin, E., Simon, I., von Heijne, G., Elofsson, A., 1997. Prediction of transmembrane alpha-helices in prokaryotic membrane proteins: the dense alignment surface method. Protein Eng. 10, 673–676.

Genoves, A., Pallas, V., Navarro, J.A., 2011. Contribution of topology determinants of a viral movement protein to its membrane association, intracellular traffic, and viral cell-to-cell movement. J. Virol. 85, 7797–7809.

Grangeon, R., Jiang, J., Laliberté, J.F., 2012. Host endomembrane recruitment for plant RNA virus replication. Curr. Opin. Virol. 2, 683–690.

Held, M.A., Boulaflous, A., Brandizzi, F., 2008. Advances in fluorescent protein-based imaging for the analysis of plant endomembranes. Plant Physiol. 147, 1469–1481.

Hofman, K., 1993. TMBASE – a database of membrane spanning protein segments. Biol. Chem. Hoppe-Seyler 374, 166–171.

Isler, J.A., Skalet, A.H., Alwine, J.C., 2005. Human cytomegalovirus infection activates and regulates the unfolded protein response. J. Virol. 79, 6890–6899.

Isogai, M., Uyeda, I., Lee, B., 1998. Detection and assignment of proteins encoded by rice black streaked dwarf fijivirus S7, S8, S9 and S10. J. Gen. Virol. 79, 1487–1494.

Jia, D., Guo, N., Chen, H., Akita, F., Xie, L., Omura, T., Wei, T., 2012. Assembly of the viroplasm by viral non-structural protein Pns10 is essential for persistent infection of *rice ragged stunt virus* in its insect vector. J. Gen. Virol. 93, 2299–2309.

Juretić, D., Lee, B., Trinajstić, N., Williams, R.W., 1993. Conformational preference functions for predicting helices in membrane proteins. Biopolymers 33, 255–273.
Laliberté, J.F., Sanfaçon, H., 2010. Cellular remodeling during plant virus infection. Annu. Rev. Phytopathol. 48, 69–91.
Liebe, S., Menzel, D., 1995. Actomyosin-based motility of endoplasmic reticulum and chloroplasts in Vallisneria mesophyll cells. Biol. Cell 85, 207–222.
Liu, H., Wei, C., Zhong, Y., Li, Y., 2007. *Rice black-streaked dwarf virus* outer capsid protein P10 has self-interactions and forms oligomeric complexes in solution. Virus Res. 127, 34–42.
Liu, L., Westler, W.M., den Boon, J.A., Wang, X., Diaz, A., Steinberg, H.A., Ahlquist, P., 2009. An amphipathic alpha-helix controls multiple roles of *brome mosaic virus* protein 1a in RNA replication complex assembly and function. PLoS Pathog. 5, e1000351.
Lu, Y., Yan, F.E.I., Guo, W.E.I., Zheng, H., Lin, L.I.N., Peng, J., Adams, M.J., Chen, J., 2011. *Garlic virus X* 11-kDa protein granules move within the cytoplasm and traffic a host protein normally found in the nucleolus. Mol. Plant Pathol. 12, 666–676.
Maass, D., Atkinson, P., 1994. Retention by the endoplasmic reticulum of rotavirus VP7 is controlled by three adjacent amino-terminal residues. J. Virol. 68, 366–378.
Nelson, B.K., Cai, X., Nebenführ, A., 2007. A multicolored set of in vivo organelle markers for co-localization studies in Arabidopsis and other plants. Plant J. 51, 1126–1136.
Peremyslov, V.V., Pan, Y.-W., Dolja, V.V., 2004. Movement protein of a closterovirus is a type iii integral transmembrane protein localized to the endoplasmic reticulum. J. Virol. 78, 3704–3709.
Reinisch, K., Nibert, M., Harrison, S., 2000. Structure of the reovirus core at 3.6 Å resolution. Nature 404, 960–967.
Schaad, M.C., Jensen, P.E., Carrington, J.C., 1997. Formation of plant RNA virus replication complexes on membranes: role of an endoplasmic reticulum-targeted viral protein. EMBO J. 16, 4049–4059.
Smith, J.A., Schmechel, S.C., Raghavan, A., Abelson, M., Reilly, C., Katze, M.G., Kaufman, R.J., Bohjanen, P.R., Schiff, L.A., 2006. Reovirus induces and benefits from an integrated cellular stress response. J. Virol. 80, 2019–2033.
Sparkes, I.A., Frigerio, L., Tolley, N., Hawes, C., 2009. The plant endoplasmic reticulum: a cell-wide web. Biochem. J. 423, 145–155.
Su, H.L., Liao, C.L., Lin, Y.L., 2002. Japanese encephalitis virus infection initiates endoplasmic reticulum stress and an unfolded protein response. J. Virol. 76, 4162–4171.
Sun, Z., Zhang, S., Xie, L., Zhu, Q., Tan, Z., Bian, J., Sun, L., Chen, J., 2013. The secretory pathway and the actomyosin motility system are required for plasmodesmatal localization of the P7-1 of *rice black-streaked dwarf virus*. Arch. Virol. 158, 1055–1064.
Trask, S.D., McDonald, S.M., Patton, J.T., 2012a. Structural insights into the coupling of virion assembly and rotavirus replication. Nat. Rev. Microbiol. 10, 165–177.
Trask, S.D., Ogden, K.M., Patton, J.T., 2012b. Interactions among capsid proteins orchestrate rotavirus particle functions. Curr. Opin. Virol. 2, 373–379.
Trujillo-Alonso, V., Maruri-Avidal, L., Arias, C.F., Lopez, S., 2011. Rotavirus infection induces the unfolded protein response of the cell and controls it through the nonstructural protein NSP3. J. Virol. 85, 12594–12604.
Tusnady, G.E., Simon, I., 2001. The HMMTOP transmembrane topology prediction server. Bioinformatics 17, 849–850.
Verchot, J., 2011. Wrapping membranes around plant virus infection. Curr. Opin. Virol. 1, 388–395.
Voinnet, O., Lederer, C., Baulcombe, D.C., 2000. A viral movement protein prevents spread of the gene silencing signal in *Nicotiana benthamiana*. Cell 103, 157–167.
Wienecke, K., Glas, R., Robinson, D.G., 1982. Organelles involved in the synthesis and transport of hydroxyproline-containing glycoproteins in carrot root discs. Planta 155, 58–63.
Xu, A., Bellamy, A.R., Taylor, J.A., 1998. BiP (GRP78) and endoplasmin (GRP94) are induced following rotavirus infection and bind transiently to an endoplasmic reticulum-localized virion component. J. Virol. 72, 9865–9872.
Ye, C.-M., Chen, S., Payton, M., Dickman, M.B., Verchot, J., 2013. TGBp3 triggers the unfolded protein response and SKP1-dependent programmed cell death. Mol. Plant Pathol. 14, 241–255.
Ye, C., Dickman, M.B., Whitham, S.A., Payton, M., Verchot, J., 2011. The unfolded protein response is triggered by a plant viral movement protein. Plant Physiol. 156, 741–755.
Zhang, G., Sanfaçon, H., 2006. Characterization of membrane association domains within the *tomato ringspot nepovirus* X2 protein, an endoplasmic reticulum-targeted polytopic membrane protein. J. Virol. 80, 10847–10857.
Zhang, H., Chen, J., Lei, J., Adams, M.J., 2001. Sequence analysis shows that a dwarfing disease on rice, wheat and maize in china is caused by *rice black-streaked dwarf virus*. Eur. J. Plant Pathol. 107, 563–567.
Zhang, L., Wang, A., 2012. Virus-induced ER stress and the unfolded protein response. Front. Plant Sci. 3, 293.
Zhang, S.C., Zhang, G., Yang, L., Chisholm, J., Sanfaçon, H., 2005. Evidence that insertion of *tomato ringspot nepovirus* NTB-VPg protein in endoplasmic reticulum membranes is directed by two domains: a C-terminal transmembrane helix and an N-terminal amphipathic helix. J. Virol. 79, 11752–11765.